Fourier-domain study of drift turbulence driven sheared flow in a laboratory plasma

M. Xu,[1,2] G. R. Tynan,[1,2] C. Holland,[1,2] Z. Yan,[2,3] S. H. Muller,[1,2] and J. H. Yu[2]
[1]*Center for Momentum Transport and Flow Organization, University of California-San Diego, La Jolla, California 92093, USA*
[2]*Center for Energy Research, University of California-San Diego, La Jolla, California 92093, USA*
[3]*Department of Engineering Physics, University of Wisconsin-Madison, Madison, Wisconsin 53706, USA*

(Received 1 December 2009; accepted 28 January 2010; published online 26 March 2010)

Frequency-resolved nonlinear internal and kinetic energy transfer rates have been measured in the Controlled Shear Decorrelation Experiment (CSDX) linear plasma device using a recently developed technique [Xu *et al.*, Phys. Plasmas **16**, 042312 (2009)]. The results clearly show a net kinetic energy transfer into the zonal flow frequency region, consistent with previous time-domain observations of turbulence-driven shear flows [Tynan *et al.*, Plasma Phys. Controlled Fusion **48**, S51 (2006)]. The experimentally measured dispersion relation has been used to map the frequency-resolved energy transfer rates into the wave number domain, which shows that the shear flow drive comes from midrange ($k_\theta \rho_S > 0.3$) drift fluctuations, and the strongest flow drive comes from $k_\theta \rho_S \approx 1$ fluctuations. Linear growth rates have been inferred from a linearized Hasegawa–Wakatani model [Hasegawa *et al.*, Phys. Fluids **22**, 2122 (1979)], which indicates that the $m=0$ mode is linearly stable and the $m=1-10$ modes (corresponding to $k_\theta \rho_S > 0.3$) are linearly unstable for the $n=1$ and $n=2$ radial eigenmodes. This is consistent with our energy transfer measurements. © *2010 American Institute of Physics*.
[doi:10.1063/1.3325397]

I. INTRODUCTION

Turbulent nonlinear energy transfer is important since it is directly related to questions of how plasma fluctuation energy is redistributed and how large scale structures, e.g., zonal flows are formed. Great efforts[1–7] have been put into this issue ever since Ritz *et al.*[8] experimentally measured the nonlinear energy transfer using a one-field model. Because it is difficult to measure plasma potential in large tokamaks (especially when a large number of spatial channels are needed) linear plasma machines become ideal devices to study the nonlinear dynamics involving turbulence and shear flows. Earlier work[9] in the Controlled Shear Decorrelation Experiment (CSDX) device suggested that turbulent energy is nonlinearly coupled to the linearly stable low k_θ zonal flow region, and further time-domain investigations by Tynan *et al.*[2] and Holland *et al.*[3] provided direct experimental support for the drift-turbulence-driven mechanism of zonal flows in this plasma. In that work, the experimentally measured Reynolds stress was used in a turbulent azimuthal momentum conservation analysis, which produced a time-averaged azimuthal velocity profile that agrees reasonably well with experimental measurements. The dynamic interplay between zonal flows and drift turbulence has also been studied in detail by Yan *et al.*,[10] which showed that a slow variation in the shear flow is accompanied by a corresponding variation in the Reynolds stress.

In this paper we report the results from a direct nonlinear energy transfer measurement based on a newly developed technique,[1] which gives a frequency domain measurement of the nonlinear convective terms in the continuity and momentum equations. These measured nonlinear energy transfer rates were then mapped into the azimuthal wave number domain using experimentally measured dispersion relation. The results show clearly a net energy transfer from the linearly unstable drift wave turbulence region with intermediate frequencies to both low frequency and high frequency regions. A comparison to linear stability of drift waves is also reported here. The content of this paper is deeply related to the issue of turbulent transport in magnetically confined fusion as seen in Refs. 11–16.

The structure of this paper is arranged as the following: Sec. II is a description of the experimental setup; Sec. III shows the detailed nonlinear energy transfer measurement; Sec. IV shows results from the linear eigenmode analysis; and finally Sec. V gives a summary and some discussions.

II. EXPERIMENTAL SETUP

As discussed in our earlier work,[1] by Fourier transforming momentum and continuity equations, ensemble-averaged energy transport equations for the spectra of density and potential fluctuations can be derived in frequency domain, where the internal and kinetic energy transfer rates come from convective derivatives $\vec{u}\cdot\nabla n$ and $\vec{u}\cdot\nabla\vec{u}$, and are defined, respectively, as

$$T_n(f,f_1) \equiv -\mathrm{Re}\langle n_f^*(\vec{u}_{\perp f_2}\cdot\nabla_\perp)n_{f_1}\rangle = -\mathrm{Re}\langle n_f^*(\hat{z}\times\nabla_\perp\phi_{f_2}\cdot\nabla_\perp)n_{f_1}\rangle, \quad (1)$$

$$T_u(f,f_1) \equiv -\mathrm{Re}\langle \vec{u}^*_{\perp f} \cdot (\vec{u}_{\perp f_2} \cdot \nabla_\perp \vec{u}_{\perp f_1}) \rangle$$
$$= -\mathrm{Re}\langle (\hat{z} \times \nabla_\perp \phi^*_f) \cdot [(\hat{z} \times \nabla_\perp \phi_{f_2} \cdot \nabla_\perp)$$
$$(\hat{z} \times \nabla_\perp \phi_{f_1})] \rangle, \quad (2)$$

where $\langle\ \rangle$ denotes the ensemble average, the asterisk denotes the complex conjugate and $\perp$ denotes the plane perpendicular to the magnetic field. The velocity $\vec{u}_\perp$ is the $\vec{E}\times\vec{B}$ velocity defined as $\vec{u}_\perp \equiv \hat{z}\times\nabla_\perp\phi$ and $f \equiv f_1 + f_2$. From earlier work, we know that a positive (negative) $T_n(f,f_1)$ or $T_u(f,f_1)$ means that fluctuations at the frequency f gain (lose) energy from (to) frequencies f_1 and f_2 through three-wave coupling. In order to determine these two terms, the plasma density fluctuations $\tilde{n}$ and their first derivative $\nabla_\perp\tilde{n}$, as well as the potential fluctuations $\tilde{\phi}$ and their first and second derivatives $\nabla_\perp\tilde{\phi}$ and $\nabla^2_\perp\tilde{\phi}$ need to be experimentally measured. These measurements were performed with a dual 3×3 probe array centered at the same radial location.[1] These quantities were then Fourier transformed into the frequency domain to compute the corresponding convolutions and finally ensemble-averaged over a sufficient number of realizations to reach statistically converged bispectra.

The experiments were carried out on a cylindrical plasma machine CSDX at the University of California, San Diego. This machine is 3 m long with a vacuum chamber radius of 10 cm. The magnetic field is produced by a series of solenoidal coils and can be continuously adjusted from 0 up to 1000 G. The plasma in this machine is produced by an $m=0$ half-wavelength helicon plasma source operating at 13.56 MHz, which produces an on-axis argon plasma density of $\sim 10^{13}$ cm^{-3} and an on-axis electron temperature of ~ 3 eV when operated at a pressure of 3.0 mTorr, magnetic field 1000 G, and rf source power 1.5 kW. More details about this machine and its basic plasma profiles, the transition to a state of weak turbulence, as well as the time-domain turbulence-driven shear flow studies on this machine can be found elsewhere.[2,9]

The dual 3×3 Langmuir probe array was installed at $z=75$ cm (here $z=0$ is defined as the interface between the source bell jar and the vacuum chamber) on this machine which enables the simultaneous measurement of plasma density and potential fluctuations and their corresponding first and second derivatives in both radial and azimuthal directions. The output analog signals from the probe array are simultaneously sampled and stored at a high time resolution (500 kHz).The measurement circuits have sufficiently high bandwidth such that for the drift turbulence signals (<25 kHz) the phase shifts introduced by the circuits are negligibly small ($<0.5°$). The 3×3 array for density channels and the 3×3 array for potential channels were centered at the same spatial point in both azimuthal and radial directions, but shifted by 1.5 mm along the magnetic field line. Since the turbulent correlation length along magnetic field line is much larger than 1.5 mm, the resulting phase shifts are also negligible. The machine runs in a steady state, which makes the measurement of long time sequences possible to achieve statistically converged bispectra.

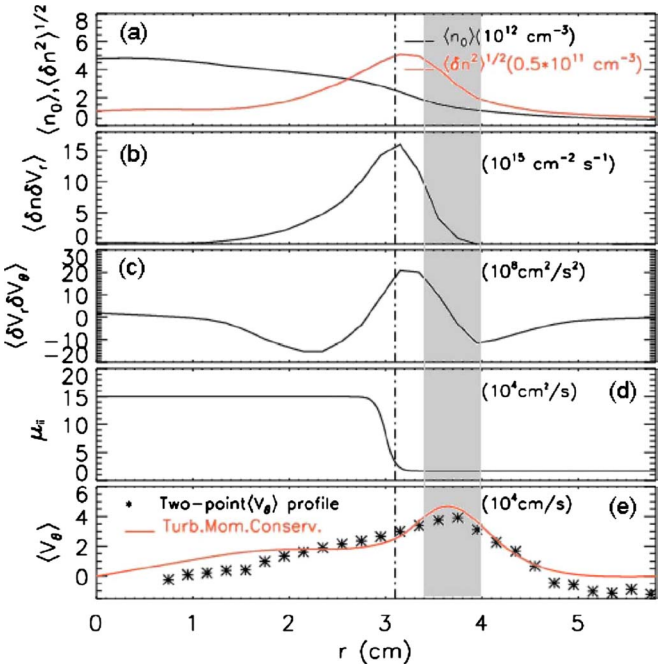

FIG. 1. (Color online) Equilibrium radial profiles for CSDX. (a) Time-averaged density (solid black) and RMS of density fluctuation (light gray/solid red). (b) Time-averaged turbulent particle flux. (c) Time-averaged Reynolds stress. (d) Estimated ion viscosity. (e) Plasma azimuthal velocity. [Reprinted with permission from Z. Yan, J. H. Yu, C. Holland, M. Xu, S. H. Muller, and G. R. Tynan, Phys. Plasmas 15, 092309 (2008). Copyright ©2008, American Institute of Physics.]

III. EXPERIMENTAL RESULTS

For convenience the basic profiles such as plasma density, potential, particle flux, etc., for the CSDX plasma have been reproduced here in Fig. 1. For more details about those profiles please refer to a former paper.[17]

The results shown here were measured at the plasma discharge condition: argon gas pressure 3.2 mtorr, B field 1000 G, and rf power 1.5 kW with reflected power less than 20 W, in order to allow direct comparison to previously published time-domain results.[2,3,10,17,18] As we can see from the spectra in Figs. 2(a)–2(c), the plasma at this condition is in a weak turbulent state, in which the fluctuations have a significant degree of frequency broadening but still reasonably follow the linear dispersion relation [see Figs. 6(a) and 6(b)] with coherent modes coexisting with turbulent flows. Both the density and potential spectra peak at around 5 and 10 kHz, which have been identified as $m>0$ collisional drift waves.[9] The potential and azimuthal velocity spectra also exhibit peaks at very low frequencies ($\leq 1-2$ kHz). These low frequency fluctuations are due to the slow evolution of the $m=0$ radially sheared flows.[10] The spectra of density and potential fluctuations are significantly different, and their cross correlation is significantly less than unity.[1] In particular we note that there is a peak at 2.5 kHz in density spectrum [Fig. 2(a)] but not in the potential spectrum [Fig. 2(b)].

The nonlinear internal and kinetic energy transfer rates $T_n(f,f_1)$ and $T_u(f,f_1)$, shown by Eqs. (1) and (2), have been measured using a dual 3×3 probe array at argon pressure 3.2 mTorr and magnetic field 1000 G. The probe array was

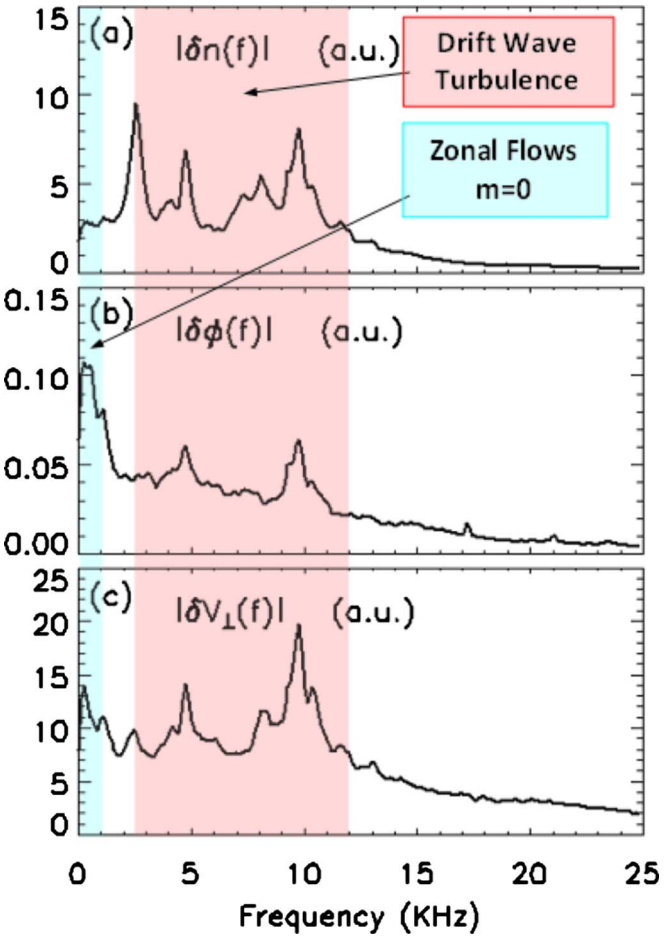

FIG. 2. (Color online) Typical autospectra (a) density, (b) potential, and (c) perpendicular velocity for the weakly turbulent plasmas in CSDX. Measurement was taken at argon pressure 3.2 mTorr, magnetic field 1000 G, and rf power 1.5 kW by the dual 3×3 Langmuir probe array centered at the radial position $r=3.6$ cm.

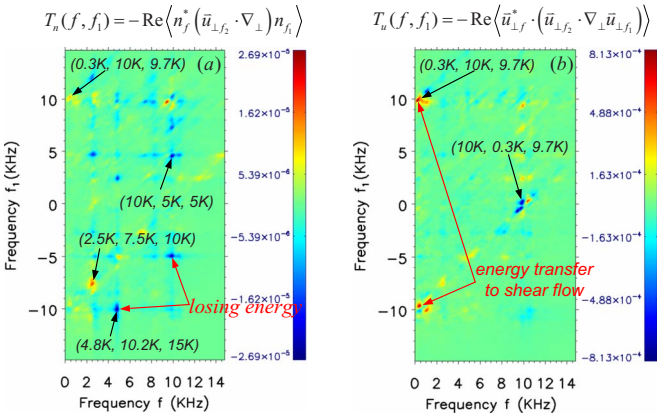

FIG. 3. (Color online) The experimentally measured nonlinear energy transfer rates. (a) Internal energy transfer. (b) Kinetic energy transfer. [Reprinted with permission from M. Xu, G. R. Tynan, C. Holland, Z. Yan, S. H. Muller, and J. H. Yu, Phys. Plasmas 16, 042312 (2009). Copyright ©2009 American Institute of Physics.] In both figures positive (negative) values correspond to a positive (negative) energy transfer to either density or perpendicular velocity fluctuations. Several prominent frequency triplets (f,f_1,f_2) are highlighted.

centered at $r=3.6$ cm, which lies at the inner radius of the shear layer [Fig. 1(e)]. About 5×10^6 sampling points on each channel were divided into roughly 1200 independent realizations to perform the bispectral calculation with good frequency resolution ($\Delta f\sim120$ Hz). It has been shown elsewhere[1] that both $T_n(f,f_1)$ and $T_u(f,f_1)$ will reasonably converge once the number of realizations reaches ~1000. For convenience, figures from that earlier paper showing the two-dimensional $T_n(f,f_1)$ and $T_u(f,f_1)$ at this discharge condition are reproduced and shown here in Fig. 3, where the positive peak at $f=0.3$ kHz and $f_1=10$ kHz in Fig. 3(b) clearly indicates that slowly varying zonal flows are coupled to drift wave turbulence and gain kinetic energy from ~10 kHz drift wave turbulences through three-wave coupling.

If we sum $T_n(f,f_1)$ over the frequency f_1, we find the net internal energy transfer rate for the frequency f, i.e., $T_n(f)=\Sigma_{f_1}T_n(f,f_1)$, which gives the total net internal energy transfer into (or out of) frequency f from all other frequencies. Figures 4(a) and 4(b) show the net internal energy transfer and the net kinetic energy transfer respectively. Here a negative value means that frequency f is losing energy and a positive value means that it is gaining energy. We can clearly see that the drift turbulence region [which corresponds to several kilohertz to ~12 kHz (Ref. 9)] loses internal and kinetic energy to both low and high frequencies. The large positive peak in the low frequency region ($f<2$ kHz) in Fig. 4(b), which has been shown to correspond to $m=0$ zonal flows [see Fig. 2(b)], gain net kinetic energy, while the large negative peak at $f\sim10$ kHz shows that fluctuation at this frequency loses kinetic energy. An examination of $T_u(f,f_1)$ in Fig. 3(b) shows that the nonlinear zonal flow drive is dominated by the transfer of energy from these 10 kHz drift fluctuations. It can be inferred that the strongest flow drive comes from $k_\theta\rho_S\approx1$ fluctuations since the 10 kHz fluctua-

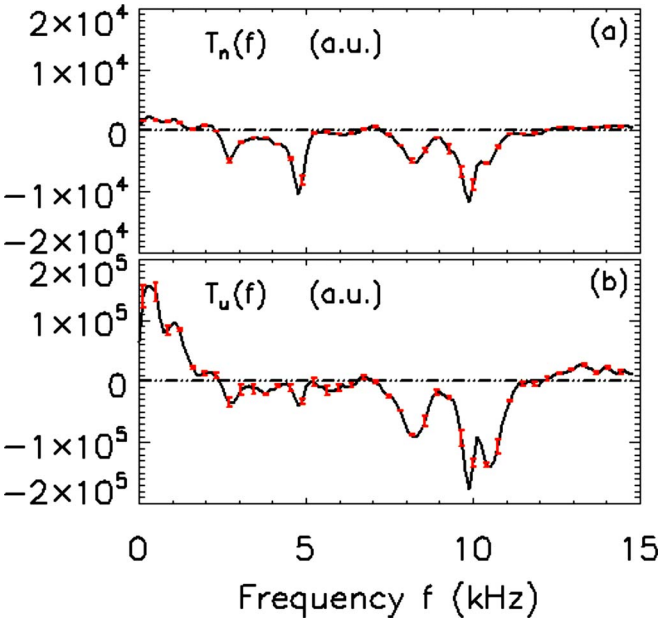

FIG. 4. (Color online) Net energy transfer rates (a) internal and (b) kinetic. Here a positive value at one specific frequency means that density (or perpendicular velocity) fluctuation at this frequency gains energy, while a negative value means losing energy.

tions can be mapped to an $m=3$ mode using the experimentally measured dispersion relation in Fig. 6(b), and for the $m=3$ mode $k_\theta = m/r \sim 0.8$ cm^{-1} and $\rho_s \sim 1$ cm.

Since the total normalized fluctuation energy in the system can be defined as $E_{\text{total}} \equiv |\tilde{n}(f)|^2 + |\tilde{u}_\perp(f)|^2$ and the internal and kinetic energy transfer rates quantitatively indicate the amount of energy redistributed among different frequencies through nonlinear processes, it is useful to sum the internal and kinetic energy transfer rates to get a net rate of the total fluctuation energy transfer, $T_{\text{total}}(f) \equiv T_n(f) + T_u(f)$. The bispectral results show that generally the magnitude of kinetic energy transfer rate is at least a factor of 5 bigger than that of the internal energy transfer rate. With Figs. 4(a) and 4(b) this means that the total energy transfer rate follows the kinetic energy transfer rate and the bulk of the total fluctuation energy is nonlinearly transferred to low frequency zonal flow region. This could be understood by noting that the total fluctuation energy can be rewritten as

$$E_{\text{total}} \sim \left(\left| \frac{\tilde{n}(r)}{n_0(r)} \right|^2 + k_\perp^2 \rho_s^2 \left| \frac{\tilde{\phi}(r)}{k_B T_{e0}(r)} \right|^2 \right),$$

and in our experiment $\rho_s = C_s/\Omega_{ci} \sim 1$ cm. At the shear layer for the $m=3$ mode $k_\theta = m/r \sim 0.8$ cm^{-1} and $k_r \gg k_\theta$ since the measured turbulence correlation length in azimuthal direction is roughly a factor of 3 higher than the turbulence correlation length in radial direction at the shear region.[17] We thus estimate that $k_\perp \rho_s \sim 3$. In our experiment the locally normalized density and potential fluctuations are about the same magnitude, i.e,

$$\left| \frac{\tilde{n}(r)}{n_0(r)} \right| \sim \left| \frac{\tilde{\phi}(r)}{k_B T_{e0}(r)} \right|.$$

Combining the above we then find that the kinetic fluctuation energy is roughly a factor of 10 higher than the density fluctuation energy. This is consistent with the measured results showing that the nonlinear kinetic energy transfer rate is much bigger than the internal energy transfer rate.

From Eqs. (1) and (2), we can see that the internal and kinetic energy transfer terms can both be divided into parts. For example $T_u(f,f_1)$ is comprised of four different parts $-\text{Re}\langle u_{y,f}^* u_{x,f_2} (\partial u_{y,f_1}/\partial x)\rangle$, $-\text{Re}\langle u_{y,f}^* u_{y,f_2} (\partial u_{y,f_1}/\partial y)\rangle$, $-\text{Re}\langle u_{x,f}^* u_{x,f_2} (\partial u_{y,f_1}/\partial y)\rangle$, and $-\text{Re}\langle u_{x,f}^* u_{y,f_2} (\partial u_{x,f_1}/\partial y)\rangle$. A similar set of expressions can be written for $T_n(f,f_1)$. By calculating each part separately and summing the resulting bispectra over f_1, the contribution from each part to the total net energy transfer rate can be found. The results of this calculation are shown in Figs. 5(a) and 5(b). The net internal energy transfer [Fig. 5(a)] shows that the term $-\text{Re}\langle n_f^* u_{x,f_2} (\partial n_{f_1}/\partial x)\rangle$ (red dash) closely follows the total internal energy transfer (solid black line), while the term $-\text{Re}\langle n_f^* u_{y,f_2} (\partial n_{f_1}/\partial y)\rangle$ (blue dot) is much smaller. This means that the term $-\text{Re}\langle n_f^* u_{x,f_2} (\partial n_{f_1}/\partial x)\rangle$ (corresponding to a radially directed $\vec{E}\times\vec{B}$ velocity interacting with a radial density gradient) is the major player for redistributing internal energy among different frequencies via nonlinear wave-wave coupling.

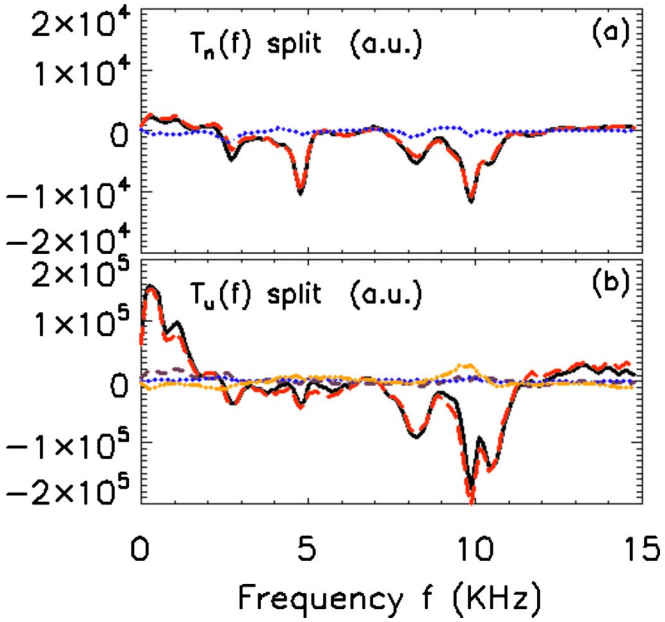

FIG. 5. (Color online) (a) Contributions to the net internal energy transfer rate due to $-\text{Re}\langle n_f^* u_{x,f_2} (\partial n_{f_1}/\partial x)\rangle$ (red dash) and $-\text{Re}\langle n_f^* u_{y,f_2} (\partial n_{f_1}/\partial y)\rangle$ (blue dot). The total value is indicated by the solid black line. (b) Contributions to the net kinetic energy transfer rate due to $-\text{Re}\langle u_{y,f}^* u_{x,f_2} (\partial u_{y,f_1}/\partial x)\rangle$ (red long dash), $-\text{Re}\langle u_{y,f}^* u_{y,f_2} (\partial u_{y,f_1}/\partial y)\rangle$ (purple short dash), $-\text{Re}\langle u_{x,f}^* u_{x,f_2} (\partial u_{y,f_1}/\partial y)\rangle$ (blue dot), and $-\text{Re}\langle u_{x,f}^* u_{y,f_2} (\partial u_{x,f_1}/\partial y)\rangle$ (orange dash dot).The total kinetic energy transfer rate is indicated by the solid black line.

We can also see in Fig. 5(b) that the term $-\text{Re}\langle u_{y,f}^* u_{x,f_2} (\partial u_{y,f_1}/\partial x)\rangle$ dominates the net kinetic energy transfer. Because $\partial \tilde{u}_y(t)/\partial x$ is the azimuthal flow shearing rate, it is clear that the slowly varying azimuthal velocity oscillations $u_y(f)$ at $f=200-300$ Hz gains energy due to the interaction between $\tilde{u}_x(t)$ at frequency $f_2 = f - f_1$ and the azimuthal shearing rate at frequency f_1. By noting that vorticity can be written as

$$\nabla_\perp^2 \phi(t) = \frac{\partial^2 \phi(t)}{\partial x^2} + \frac{\partial^2 \phi(t)}{\partial y^2},$$

and that

$$\left| \frac{\partial^2 \tilde{\phi}(t)}{\partial x^2} \right| \gg \left| \frac{\partial^2 \tilde{\phi}(t)}{\partial y^2} \right|,$$

in our experiments, we can take $\partial^2 \tilde{\phi}(t)/\partial x^2$ approximately to be vorticity, and hence $\tilde{u}_x(t)(\partial \tilde{u}_y(t)/\partial x) = \tilde{u}_x(t)(\partial^2 \tilde{\phi}(t)/\partial x^2) \approx \tilde{u}_x(t) \nabla_\perp^2 \tilde{\phi}(t)$ is approximately the instantaneous radial flux of vorticity. This result then suggests that one can also view the shear flow as being generated by a flux of vorticity which accumulates at the shear layer and reinforces or amplifies the shear flow. By noting that, for divergence-free flows such as $\vec{E}\times\vec{B}$ drifts, we can write $\partial \langle \tilde{u}_x \tilde{u}_y \rangle / \partial x = \langle \tilde{u}_x \tilde{\omega}_z \rangle$, where $\tilde{\omega}_z \equiv (\nabla \times \tilde{u})_z$ is the vorticity of the fluctuating velocity in the x-y plane;[19,20] this interpretation can be seen to be entirely consistent with the results of Holland *et al.*,[3] which showed that the time-averaged Reynolds stress was consistent with the observed shear flow profile and estimated damping processes. The results here show that the transient vorticity flux $\tilde{u}_x(t)[\partial^2 \tilde{\phi}(t)/\partial x^2]$ is responsible for the transfer of turbulent

energy in frequency space, and specifically is responsible for the transfer of turbulent momentum with higher frequency into shear flows with lower frequency at the shear layer. This result provides a consistent and complementary picture of the fluctuations drive mechanism of shear flows to the earlier time-domain picture which attributes the shear flow drive to an accumulation of turbulent momentum within the shear layer.

IV. LINEAR STABILITY ANALYSIS WITH COMPARISON TO EXPERIMENT

The idea that (usually linearly) unstable modes release free energy into finite amplitude fluctuations, and the energy of these fluctuations is then nonlinearly transferred into stable fluctuations is assumed in nearly all turbulence models (see e.g., the Hasegawa–Wakatani collisional drift-wave model[21]). We can compare our results with linear stability analysis in order to provide a test of this model. We proceed by first assuming that the equilibrium density is of Gaussian form $n_0(r)=n_0 \exp(-0.5(r/L_n)^2)$ [which is close to the profile shown in Fig. 1(a)].With this profile in the linearized Hasegawa–Wakatani collisional drift turbulence model (thought to be appropriate for this experiment) in a cylindrical geometry, we find the linear dispersion relation

$$-ik_{mn}^2\omega_{mn}^2+[\omega_{\|}(1+k_{mn}^2)+\nu_k]\omega_{mn}-\omega_{\|}\left(m\frac{\rho_s}{L_n}-i\nu_k\right)=0. \tag{3}$$

Here k_{mn} is the effective radial wave number denoted by $k_{mn}=X_{mn}/a$, where X_{mn} is the nth zero of $J_m(x)$ and a is the radius of the plasma cylinder. $\omega_{\|}=k_{\|}^2 v_{Te}^2/\nu_{ei}$ is the parallel electron adiabatic parameter (assumed constant here) and $\nu_k=(\nu_{i-n}+\mu_{ii}k_{mn}^2)k_{mn}^2$ is a dimensionless measure of perpendicular dissipation due to the combined effect of the ion-neutral collision frequency ν_{i-n} and the ion-ion collisional viscosity. More details about this calculation can be found elsewhere.[22] By using typical CSDX parameters for the 1000 G case with an average electron temperature $T_e \sim 2.0$ eV, density gradient scale length $L_n \sim 2.5$ cm, plasma radius $a=10.0$ cm, an average ion neutral collision rate $\nu_{i-n} \sim 6.0$ kHz, and an average ion collisional viscosity $\mu_{ii} \sim 2.0\times 10^4$ cm^2/s,[3] we can solve the complex eigenfrequencies ω_{mn} from the linear dispersion relation and thus find the real frequencies and the growth rates for each eigenmode. The Doppler shift introduced by the mean $\vec{E}\times\vec{B}$ flow associated with the azimuthal flow has been taken into account by adding a frequency shift given by $k_\theta\langle V\rangle_\theta$, where the value of $\langle V_\theta\rangle$ measured by a Mach probe[18] was used. This Doppler shifted frequency ω_{mn} (real part) for $n=1$ is shown as the black dashed line in Fig. 6(a), where the calculated dispersion agrees well with the experimentally measured dispersion relation at the strong density gradient region. Note that in these figures the effective azimuthal mode number, m_{eff}, is a continuous variable defined as $m_{\text{eff}}=k_\theta r$.

By using two azimuthally separated Langmuir probes, the spectrum $S(f,k_\theta)$ can be measured and a mapping between frequencies and azimuthal mode numbers can be established.[23] Figure 6(a) shows the two-point k-spectrum

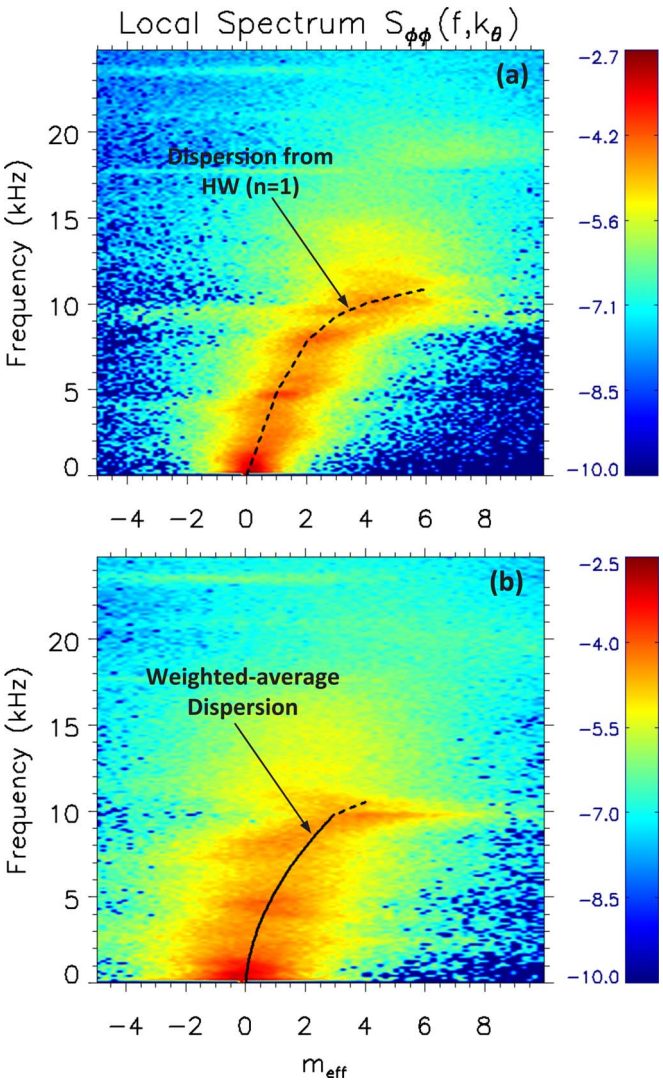

FIG. 6. (Color online) Two-point spectrum $S(f,k_\theta)$ from potential (with the intensity in log scale). (a) Dispersion measured at $r=2.6$ cm (strong density gradient region) and the black dashed line is for the real part of the linear eigenmode frequencies of the first radial eignemode branch ($n=1$) calculated from the linear dispersion relation Eq. (3) with Doppler shift accounted (using typical CSDX parameters $T_e \sim 2.0$ eV, $L_n \sim 2.5$ cm, $a=10.0$ cm, $\nu_{i-n} \sim 6.0$ kHz, and $\mu_{ii} \sim 2.0\times 10^4$ cm^2/s). The effective azimuthal mode number is a continuous variable defined as $m \equiv k_\theta r$. (b) Dispersion measured at $r=3.6$ cm (maximum shear region), and the black solid line indicates the weighted-average values, which were used to map the nonlinear transfer rate in the frequency space into the wave number space.

measured at $r=2.6$ cm at the strong density gradient region, where the x-axis is the azimuthal mode number and the y-axis is frequency. Figure 6(b) is the dispersion relation measured at $r=3.6$ cm at the maximum shear region. We can see that the spectrum exhibits strong dispersion for $m \geq 3$, and several azimuthal mode numbers $m \sim 3$–6 are degenerate with frequency $f \sim 10$ kHz. It is interesting to note that the strong nonlinear interaction of these degenerate fluctuations is what leads to the very low frequency ($f \sim 200$–300 Hz) $m=0$ sheared flow fluctuation (shown in Fig. 2); this observation may be the $m=0$ limit of the more general nonlinear convective cell generation mechanism discussed by Shukla.[24]

With the experimentally measured k-spectrum in

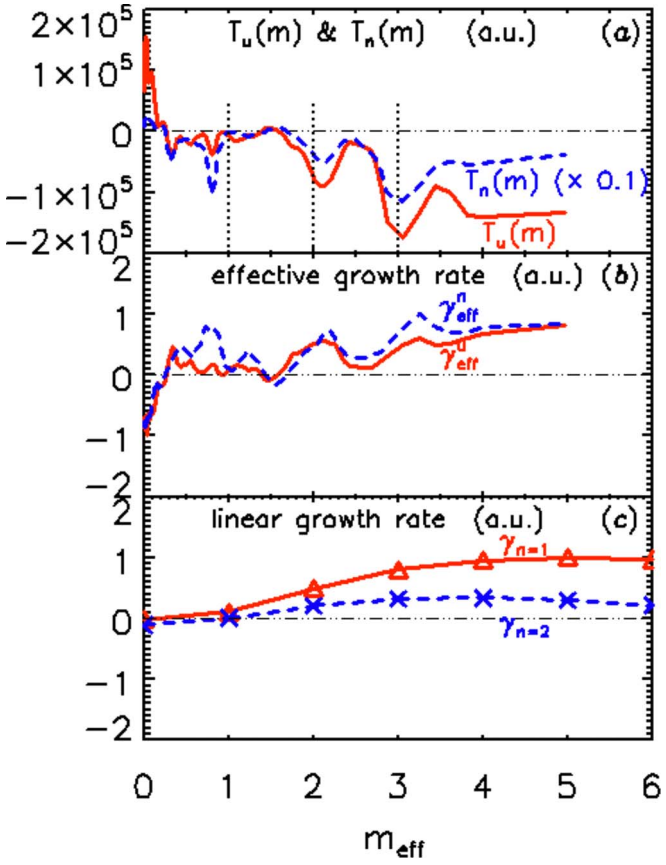

FIG. 7. (Color online) (a) Nonlinear energy transfer rates mapped from frequency domain to wave number domain using the experimentally measured k-spectrum $S(f,k_\theta)$ presented in Fig. 6(b). The red solid line is for $T_u(m)$ and the blue dashed line is for $T_n(m)$. (b) Effective growth rates inferred from the nonlinear net energy transfer rates. The red solid line is for γ^μ_{eff} and the blue dashed line is for γ^n_{eff}. (c) Linear growth rates from Hasegawa–wakatani model. The red solid line is the growth rate of the first linear radial eigenmode $n=1$, $\gamma_{n=1}$, and the blue dashed line is for the second radial eigenmode $n=2$, $\gamma_{n=2}$.

Fig. 6(b), we can now map the measured energy transfer rates from the frequency domain to the azimuthal wave number domain. To do this, for each frequency a weighted-average value $\bar{k}_\theta(f) \equiv \int_0^\infty S(f,k_\theta)k_\theta dk_\theta / \int_0^\infty S(f,k_\theta)dk_\theta$ was obtained by averaging over the two-point spectrum in Fig. 6(b), then those values for different frequencies were smoothed to get the black solid line in Fig. 6(b). The resulting effective curve $F(\bar{k}_\theta)$ was used to map the net energy transfer rates into the wave number domain. Figure 7(a) shows the mapped kinetic energy transfer rate $T_u[\bar{k}_\theta(f)]$ by the red solid curve and the mapped internal energy transfer rate $T_n[\bar{k}_\theta(f)]$ by the blue dashed line. The results show that the zonal flow ($m \sim 0$ mode) gains net kinetic energy while fluctuations with $m=1,2,3$, etc. lose kinetic energy. The mapping for $m \geq 4$ has large uncertainties when the mapping frequencies approach ~ 10 kHz due to the frequency degeneracy seen in Fig. 6(b). However it is still very clear from Fig. 6(b) that the major zonal flow driving frequency range of 9–11 kHz corresponds to azimuthal modes $m \geq 3$, implying that the kinetic energy carried by fluctuations with higher azimuthal wave number is nonlinearly transferred to $m \sim 0$ mode where it is (presumably) damped away through collisional processes. The driving source for those waves with higher azimuthal mode numbers still needs to be identified. As we show next, the $m=1-10$ modes are linearly unstable thus they can tap energy directly from density gradient; in addition they can interact nonlinearly with each other to rearrange the energy spectrum.

In Fig. 6(a), the real parts of the linear eigenfrequencies for the first radial eigenmode were plotted as the black dashed line, which agrees well with the experimentally measured k-spectrum. The imaginary parts of the linear eigenfrequencies (i.e., the linear growth rates) for the first and second radial eigenmodes were plotted in Fig. 7(c). We find that the $m \geq 1$ modes on the $n=1$ and $n=2$ branches are both linearly unstable. Furthermore, we note that the unstable (stable) regions correspond to the regions where $T_u < 0$ ($T_u > 0$), consistent with expectations for a stationary spectrum established by balancing the linear growth/decay against the nonlinear energy transfer. To test the consistency of this spectrum balance picture, we can lump the linear effects into an effective linear growth/damping rate γ^μ_{eff} and rewrite the frequency-domain kinetic energy transport equation (see Ref. 1) as

$$\left\langle \frac{1}{2}\frac{\partial |\vec{u}_{\perp f}|^2}{\partial t} \right\rangle = T_u(f) + \gamma^\mu_{\text{eff}}(f)\langle |\vec{u}_{\perp f}|^2 \rangle. \tag{4}$$

For a time stationary plasma, the left-hand side of the Eq. (4) is zero. By dividing the equation by $\langle |\vec{u}_{\perp f}|^2 \rangle$ we can infer an effective linear growth/damp rate as $\gamma^\mu_{\text{eff}}(f) \equiv -T_u(f) / \langle |\vec{u}_{\perp f}|^2 \rangle$, which can be compared to the analytically calculated linear grow rate from Eq. (3). The red solid line in Fig. 7(b) shows the result. We note that this effective growth rate is consistent with the linear stability analysis. The sign of γ^μ_{eff} agrees with the linear stability analysis, and the relative magnitude of the unstable region, where $\gamma^\mu_{\text{eff}} > 0$ and where $\gamma_{n=1} > 0$ and $\gamma_{n=2} > 0$, is in rough agreement. However, we also note that γ^μ_{eff} for $m_{\text{eff}} \approx 0$ is significantly more negative than $\gamma_{n=1}$ and $\gamma_{n=2}$ at $m_{\text{eff}} \approx 0$. This result, which is found by balancing the time-averaged zonal flow amplitude against the nonlinear energy transfer into the zonal flow, suggests that some additional damping mechanism, unrelated to the damping mechanism that are contained in the linear stability analysis, may influence the zonal flow saturation. Additional work is required to determine if this is the case.

V. SUMMARY AND DISCUSSION

We have shown in this paper that the directly measured nonlinear energy transfer rates for both velocity and density fluctuations are negative at intermediate frequencies and positive in both low and high frequency regions, indicating that turbulent energy is nonlinearly transferred to low frequency zonal flows and to regions at higher frequencies, where the energy is then presumably dissipated. In addition, we find that the radial flux of vorticity, equivalent to the gradient of turbulent Reynolds stress, is dominantly responsible for redistributing turbulent kinetic energy among different frequencies (or different scales).Thus the vorticity flux can be thought of as having two equivalent roles: it leads to

the transport of momentum in configuration space and to the spreading of energy among different spatiotemporal scales in the Fourier domain.

We also compared the net nonlinear transfer results against a linear eigenmode calculation based on the Hasegawa–Wakatani model. Despite the use of very simplified profiles (flat electron temperature, ion viscosity profiles, etc.), the comparison shows that the linearly unstable fluctuations correspond to the regions where the nonlinear transfer leads to a loss of energy. Conversely, the linearly stable fluctuations correspond to regions that receive nonlinearly transferred energy. Linear analysis also shows that $m \geq 1$ modes of the first two radial eigenmodes $n=1$ and $n=2$ are unstable at the typical CSDX condition, suggesting that these two radial eigenmodes could play a role in driving the zonal flows.

The observation that zonal flows are driven predominantly by the radial flux of vorticity, combined with the observation that the shear layer is spatially separated from the strong gradient region (which presumably is where drift fluctuations originate) suggests a picture, where drift fluctuations with finite vorticity are generated at one location and then propagate outward and then interact with and reinforce a pre-existing shear layer. We are currently investigating this possibility, and will report the results in a subsequent paper.

ACKNOWLEDGMENTS

One of the authors (G.R.T,) acknowledges useful discussions with P. H. Diamond. This research is performed under the U.S. Department of Energy (DOE) Grant No. DE-FG02-OER54871.

[1] M. Xu, G. R. Tynan, C. Holland, Z. Yan, S. H. Muller, and J. H. Yu, Phys. Plasmas **16**, 042312 (2009).
[2] G. R. Tynan, C. Holland, J. H. Yu, A. James, D. Nishijima, M. Shimada, and N. Taheri, Plasma Phys. Controlled Fusion **48**, S51 (2006).
[3] C. Holland, J. H. Yu, A. James, D. Nishijima, M. Shimada, N. Taheri, and G. R. Tynan, Phys. Rev. Lett. **96**, 195002 (2006).
[4] J. S. Kim, R. D. Durst, R. J. Fonck, E. Fernandez, A. Ware, and P. W. Terry, Phys. Plasmas **3**, 3998 (1996).
[5] S. J. Camargo, D. Biskamp, and B. D. Scott, Phys. Plasmas **2**, 48 (1995).
[6] P. Manz, M. Ramisch, and U. Stroth, Plasma Phys. Controlled Fusion **51**, 035008 (2009).
[7] C. Hidalgo, C. Silva, M. A. Pedrosa, E. Sanchez, H. Fernandes, and C. A. F. Verandas, Phys. Rev. Lett. **83**, 2203 (1999).
[8] C. P. Ritz, E. J. Powers, and R. D. Bengtson, Phys. Fluids B **1**, 153 (1989).
[9] M. J. Burin, G. R. Tynan, G. Y. Antar, N. A. Crocker, and C. Holland, Phys. Plasmas **12**, 052320 (2005).
[10] Z. Yan, G. R. Tynan, C. Holland, M. Xu, S. H. Muller, and J. H. Yu, Phys. Plasmas **17**, 032302 (2010).
[11] G. R. Tynan, A. Fujisawa, and G. Mckee, Plasma Phys. Controlled Fusion **51**, 113001 (2009).
[12] P. H. Diamond, C. J. McDevitt, Ö. D. Gürcan, T. S. Hahm, W. X. Wang, E. S. Yoon, I. Holod, Z. Lin, V. Naulin, and R. Singh, Nucl. Fusion **49**, 045002 (2009).
[13] C. Hidalgo, B. Gonçalves, C. Silva, M. A. Pedrosa, K. Erents, M. Hron, and G. F. Matthews, Phys. Rev. Lett. **91**, 065001 (2003).
[14] P. H. Diamond, S. I. Itoh, K. Itoh, and T. S. Hahm, Plasma Phys. Controlled Fusion **47**, R35 (2005).
[15] A. Fujisawa, K. Itoh, H. Iguchi, K. Matsuoka, S. Okamura, A. Shimizu, T. Minami, Y. Yoshimura, K. Nagaoka, C. Takahashi, M. Kojima, H. Nakano, S. Ohsima, S. Nishimura, M. Isobe, C. Suzuki, T. Akiyama, K. Ida, K. Toi, S.-I. Itoh, and P. H. Diamond, Phys. Rev. Lett. **93**, 165002 (2004).
[16] A. Fujisawa, K. Itoh, A. Shimizu, H. Nakano, S. Ohshima, H. Iguchi, K. Matsuoka, S. Okamura, T. Minami, Y. Yoshimura, K. Nagaoka, K. Ida, K. Toi, C. Takahashi, M. Kojima, S. Nishimura, M. Isobe, C. Suzuki, T. Akiyama, Y. Nagashima, S.-I. Itoh, and P. H. Diamond, Phys. Rev. Lett. **98**, 165001 (2007).
[17] Z. Yan, J. H. Yu, C. Holland, M. Xu, S. H. Muller, and G. R. Tynan, Phys. Plasmas **15**, 092309 (2008).
[18] J. H. Yu, C. Holland, G. R. Tynan, G. Antar, and Z. Yan, J. Nucl. Mater. **363–365**, 728 (2007).
[19] G. I. Taylor, Philos. Trans. R. Soc. London, Ser. A **215**, 1 (1915).
[20] P. H. Diamond, O. D. Gurcan, T. S. Hahm, K. Miki, Y. Kosuga, and X. Garbet, Plasma Phys. Controlled Fusion **50**, 124018 (2008).
[21] A. Hasegawa and C. G. Maclennan, Phys. Fluids **22**, 2122 (1979).
[22] Z. Yan, G. R. Tynan, C. Holland, M. Xu, S. H. Muller, and J. H. Yu, Phys. Plasmas **17**, 012302 (2010).
[23] J. M. Beall, Y. C. Kim, and E. J. Powers, J. Appl. Phys. **53**, 3933 (1982).
[24] P. K. Shukla, M. Y. Yu, and K. H. Spatschek, Phys. Rev. A **23**, 3247 (1981).